Article:
Barr, A.D., Tyas, A., Farrimond, D.G. et al. (2025) Fast-running thermochemical predictions of quasi-static pressure for confined detonations of plasticised high explosives. Process Safety and Environmental Protection, 202 (Part B). 107678. ISSN: 0957-5820

https://doi.org/10.1016/j.psep.2025.107678

Fast-running thermochemical predictions of quasi-static pressure for confined detonations of plasticised high explosives

Andrew D. Barr[a,b], Andy Tyas[a,b], Dain G. Farrimond[a,b], Scott Woolford[b], Tom Speak[c], Sam E. Rigby[a], Sam D. Clarke[a,b], Tommy Lodge[a,b]

[a]*School of Mechanical, Aerospace & Civil Engineering, University of Sheffield, Mappin Street, Sheffield, S1 3JD, UK*
[b]*Blastech Ltd., The Innovation Centre, 217 Portobello, Sheffield, S1 4DP, UK*
[c]*School of Mathematical and Physical Sciences, University of Sheffield, Western Bank, Sheffield, S3 7HF, UK*

Abstract

When explosives detonate in a confined space, repeated reflections of the initial shockwave lead to the development of a long-term quasi-static pressure (QSP), which can cause severe structural damage and loss of life. Mixing of the detonation products with an oxygen-rich atmosphere results in additional energy release through 'afterburn' reactions, which further increase this pressure. Government agencies tasked with protecting the public from explosive threats require tools that can quickly assess the risk posed by QSP for a range of possible scenarios. Existing empirical relationships for TNT offer rapid calculation, but have not been validated against other explosive types. Conversely, specialised CFD and thermochemical codes can accurately predict QSP development for many explosives, but are computationally expensive. Here we develop a fast-running thermochemical model for the confined detonation of RDX- and PETN-based plastic explosives. Using simplified detonation and combustion reactions for the explosive and binder,

we calculate the resulting internal energy change in the chamber atmosphere, and hence the QSP. The resulting predictions are within 3% of experimental values for both oxygenated and inert atmospheres, indicating that the contributions of detonation and afterburn to the energy release are reliably modelled. The thermochemical model is provided as a Python script which can be readily adapted for other explosives and atmospheric conditions.

Keywords:
confined explosions, quasi-static pressure, thermochemical modelling, afterburn, plastic explosives, fast-running models

---

1. Introduction

When explosives detonate in a confined space, the resulting high-pressure loading can cause severe structural damage and loss of life. In the aftermath of recent terrorist attacks in the UK, such as the '7/7' attacks in London in 2005 (56 deaths, 784 injured) and the Manchester Arena bombing in 2017 (23 deaths, 1017 injured), government agencies require quick-running tools to help them predict, and proactively prevent, the effects of explosive devices [1]. These predictive tools are designed to estimate the blast and fragmentation effects of a device in a particular location and the resulting injury distributions, and a fundamental aspect of their algorithms is the accurate prediction of the blast load itself. In confined detonations, the presence of walls and other obstacles leads to multiple reflections of the initial shock wave within the space, leading to complex shock wave interactions and the development of a long-term, uniform quasi-static pressure, or QSP. The magnitude of this

QSP is controlled by the energy and volume of gaseous products released in the detonation, and the overall volume of the space, as the overpressure depends on the temperature increase of the gases inside the fixed volume.

This process is complicated by the fact that most explosives are fuel-rich, and undergo additional combustion, or afterburn, when the fireball of detonation products interacts with oxygen in the surrounding atmosphere. These afterburn reactions release additional energy which contributes to the QSP in the space [2], but are dependent on sufficient mixing of the detonation products with atmospheric oxygen before the system cools to the point of product freeze-out [3, 4].

The simplest method of QSP prediction is through use of empirical relationships, typically relating peak QSP to the ratio of charge mass to chamber volume. Experimental work by Weibull [5], Kingery et al. [6], Kinney and Sewell [7], Esparza et al. [8] and others was used by Anderson et al. [9] to produce such an empirical relationship for TNT, which also included the effect of venting area on QSP decay. A similar method was employed to define the predictive curve within UFC 3-340-02 [10] shown in Figure 1a. This curve is based on experiments using TNT detonations in air. While the TNT equivalence of other explosives in confined detonations is not well established, UFC 3-340-02 suggests the following formula 'based on a limited amount of testing':

$$W_{\mathrm{Eg}} = \frac{\phi(H^c_{\mathrm{EXP}} - H^d_{\mathrm{EXP}}) + H^d_{\mathrm{EXP}}}{\phi(H^c_{\mathrm{TNT}} - H^d_{\mathrm{TNT}}) + H^d_{\mathrm{TNT}}} W_{\mathrm{EXP}} \tag{1}$$

where the mass of the required explosive, W_{EXP}, is converted to the equivalent mass of TNT, W_{Eg}, using a ratio of the heats of combustion and detonation of the required explosive (H^c_{EXP} and H^d_{EXP}) and of TNT (H^c_{TNT} and H^d_{TNT}).

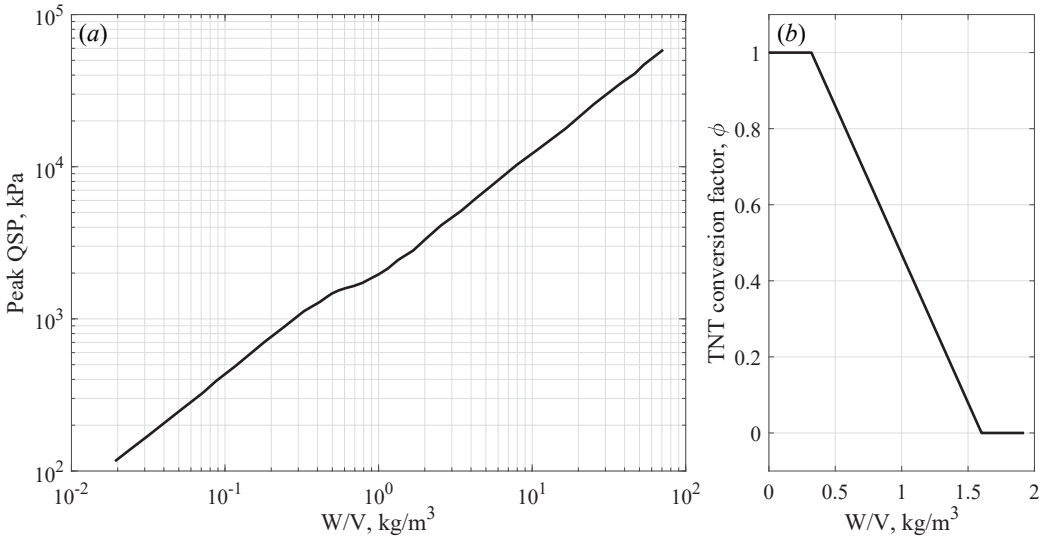

Figure 1: a) UFC 3-340-02 empirical curve for peak gas pressure produced by a TNT detonation in a partially contained chamber, and b) TNT conversion factor. Converted to SI units from [10].

An additional 'TNT conversion factor', ϕ, controls the contribution of combustion to this calculation based on the charge mass and chamber volume, as shown in Figure 1b. In the case of an air atmosphere at standard temperature and pressure, this provides a measure of the oxygen available for afterburn.

More recently, numerical methods have allowed detailed modelling of the detonation, shock propagation and interactions, and the chemical reactions between the detonation products and atmosphere [11, 12]. These methods tend to be computationally expensive, and their accuracy is dependent on how the afterburn reactions and subsequent energy release are modelled. Thermochemical analyses using codes such as CHEETAH [13] perform detailed calculations of the chemical reactions including equilibria and kinetics,

and can be used to predict the resulting pressure, temperature and gas species in a confined space [14]. These can also be effective, but are often not available to the general user, and require more detail than might be available in a real-world situation where the threat is not well defined.

Feldgun et al. [15] and Edri et al. [16] have proposed a number of semi-empirical/analytical models for the prediction of QSP, which are based on conservation of mass and energy, and an assumption of ideal gas behaviour of the detonation products. These simplified thermochemical calculations involve assuming the mean detonation and combustion reactions for the explosive, calculating the internal energy of the chamber gases following these reactions, and then the resultant increase in pressure of the new gas mixture. Following these steps for TNT, RDX, PETN and ANFO detonations in air, good agreement was observed with UFC 3-340-02 and other empirical curves over a range of charge mass to volume ratios.

Farrimond et al. [17] recently presented experimental data on the confined detonation of RDX- and PETN-based plasticised explosives in air, nitrogen and argon atmospheres, seeking to understand the effects of afterburn in explosives where the binder acts as an additional source of fuel. These experiments were highly repeatable, and independent measurements of QSP and temperature showed that assumptions of ideal gas behaviour hold, suggesting that a simplified thermochemical method could also be applied to these more complex explosive compositions.

This paper develops a fast-running thermochemical model for plastic explosive detonations in air, nitrogen and argon atmospheres, considering the contributions of detonation and the afterburn of the detonation products and

binder to the peak QSP in a confined chamber. These model predictions are validated against the experimental pressure and temperature results from Farrimond et al. [17], and an open source Python script is provided to allow other researchers to utilise and expand on these methods.

2. Plasticised explosives

This work considers the detonation of three British plasticised explosives: PE4 (Plastic Explosive No. 4), PE8, and PE10. Plasticised, or plastic, explosives are high explosives whose stability and mouldability have been enhanced through the incorporation of binding agents and plasticisers, which ensure the material is cohesive and flexible. The explosives in this study are based on RDX (PE4 and PE8) or PETN (PE10), which have oxygen balances of -21.6% and -10.1%, respectively; however, the additional fuel provided by the binder materials significantly increases their overall oxygen deficiency.

The availability of oxygen in an explosive affects the products that are produced, and the energy released, during detonation. An oxygen-balanced explosive will contain enough oxygen to fully oxidise the carbon and hydrogen in the explosive to carbon dioxide and water during detonation, and the heat energy associated with these reactions is released fully during the detonation itself. An oxygen-deficient explosive will result in incomplete oxidation and the production of carbon monoxide and other products, which may only then combust further if sufficient oxygen is present in the surrounding atmosphere, i.e. through afterburn of the detonation products [2]. The binder materials in a plastic explosive act as an additional combustible fuel, which can also oxidise and contribute to the energy release of the explosion. Common plastic

explosives are all oxygen-deficient, and so the energy release associated with the afterburn of the detonation products and the combustion of the binder materials (jointly referred to as "afterburn" from this point) only occurs after detonation, upon mixing with additional atmospheric oxygen [17].

2.1. Explosive formulations and reactions

Producing a thermochemical model for the detonation of plastic explosives requires defining the reactions that take place, and the heat of reaction associated with these. A model intended for rapid assessment of an explosive device for initial design or emergency response will typically ignore the kinetics and equilibria of these reactions in favour of temperature-independent approximations, such as the Kistiakowsky–Wilson or Springall–Roberts rules. For example, this was the approach taken by Edri et al. [16] to predict the contribution of afterburn to confined detonations of TNT, RDX and PETN. The Kistiakowsky–Wilson (K–W) rules assume the following reaction hierarchy during detonation [18]:

1. Carbon atoms are converted to carbon monoxide;
2. If any oxygen remains, then hydrogen is oxidised to water;
3. If any oxygen remains, then carbon monoxide is oxidised to carbon dioxide;
4. All the nitrogen is converted to nitrogen gas, N_2.

The K–W predictions for RDX and PETN are shown in Table 2, along with the heat of detonation associated with these reactions. The heat of detonation can be calculated using Hess's Law as the difference between the heats of formation of the explosive and the gaseous detonation products.

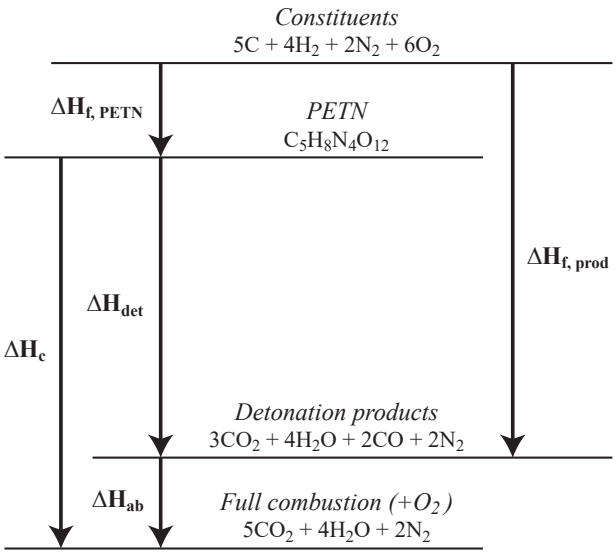

Figure 2: Enthalpy diagram for reactions involving the explosive PETN. The heat of combustion, ΔH_{c}, for full combustion of PETN in excess oxygen is equivalent to the sum of the heat of detonation, ΔH_{det}, and the heat of afterburn, ΔH_{ab}.

This is illustrated in the enthalpy diagram in Figure 2 for PETN, where the heat of detonation, ΔH_{det}, is the difference between $\Delta H_{\text{f, PETN}}$ and $\Delta H_{\text{f, prod}}$. Following the K–W rules, the detonation reaction of PETN is $C_5H_8N_4O_{12} \longrightarrow 3\,CO_2 + 4\,H_2O + 2\,CO + 2\,N_2$, and so using published values of ΔH_{f} [18],

$$\begin{aligned}
\Delta H_{\text{f, PETN}} &= -530.53 \text{ kJ/mol} \\
\Delta H_{\text{f, prod}} &= 3\Delta H_{\text{f, CO2}} + 4\Delta H_{\text{f, H2O}} + 2\Delta H_{\text{f, CO}} + 2\Delta H_{\text{f, N2}} \\
&= 3(-393.51) + 4(-241.83) + 2(-110.53) + 2(0) \\
&= -2368.90 \text{ kJ/mol} \\
\Delta H_{\text{det}} &= \Delta H_{\text{f, prod}} - \Delta H_{\text{f, PETN}} \\
&= (-2368.90) - (-530.53) \\
&= -1838.37 \text{ kJ/mol}
\end{aligned}$$

From Table 2 the molar mass of PETN is 316.138 g/mol, and so the heat of detonation can also be expressed in terms of mass as

$$\begin{aligned}
\Delta H_{\text{det}} &= -1838.37(1000)/316.138 \\
&= -5815.08 \text{ kJ/kg}
\end{aligned}$$

Hess's Law can also be used to calculate the heat of combustion, ΔH_{c}, that would be evolved if the explosive was fully oxidised, as shown in Table 3. Assuming that sufficient additional oxygen is available, in this case the reaction products are those of full combustion, $C_5H_8N_4O_{12} + O_2 \longrightarrow 5\,CO_2 + 4\,H_2O + 2\,N_2$. The heat of combustion is then the difference between the heat of formation of the reactants and products as before:

$$\Delta H_{\text{f, reac}} = \Delta H_{\text{f, PETN}} + \Delta H_{\text{f, O2}}$$

$$
\begin{aligned}
&= -530.53 + (0) = -530.53 \text{ kJ/mol} \\
\Delta H_{\text{f, prod}} &= 5\Delta H_{\text{f, CO2}} + 4\Delta H_{\text{f, H2O}} + 2\Delta H_{\text{f, N2}} \\
&= 5(-393.51) + 4(-241.83) + 2(0) \\
&= -2934.87 \text{ kJ/mol} \\
\Delta H_{\text{c}} &= \Delta H_{\text{f, prod}} - \Delta H_{\text{f, reac}} \\
&= (-2934.87) - (-530.53) \\
&= -2404.34 \text{ kJ/mol} \\
&= -7605.33 \text{ kJ/kg}
\end{aligned}
$$

The heat of afterburn, ΔH_{ab}, is then the difference between the heat of combustion and the heat of detonation, as also shown in Figure 2.

$$
\begin{aligned}
\Delta H_{\text{ab}} &= \Delta H_{\text{c}} - \Delta H_{\text{det}} \\
&= (-7605.33) - (5815.08) \\
&= -1790.26 \text{ kJ/kg}
\end{aligned}
$$

2.2. Binder formulations and reactions

Each of the plastic explosives considered in this paper are approximately 85% explosive by mass, with the balance formed of binders and plasticisers, and a small amount ($< 1\%$) of DMDNB as a taggant to aid explosive detection. The proprietary nature of plastic explosive production means that reliable information on the exact compositions is difficult to find, and there is likely variation from batch to batch. Even when the components are listed on material safety data sheets, oils and waxes are usually generically listed as such, without reference to the chain lengths of the hydrocarbons they contain.

For example, a typical MSDS for PE4 lists its composition as $> 90\%$ RDX, $< 5\%$ paraffin oil, $< 5\%$ lithium stearate and $< 1\%$ DMDNB by mass. A composition analysis on the batch of PE4 used in the current work by Speak et al. [19] indicated a composition of 81.95% RDX, 6.01% HMX, 0.96% DMDNB and 11.08% 'oils', which represents the paraffin oil, dioleate and lithium stearate components. Noting that both HMX and RDX are present as explosive components, and the complexity of the oil components, it is desirable for the purpose of a fast-running model to simplify the chemistry as much as possible: comparison with the experimental data will indicate whether these assumptions are reasonable.

Table 1 shows the simplified compositions adopted for PE4, PE8 and PE10, where in each case the explosive fraction is paired with a representative binder 'fuel' from the known ingredients, excluding DMDNB and other minor constituents. PE4 is modelled using RDX and $C_{25}H_{52}$ paraffin wax as the binder to maintain the simple CHNO chemistry of the K–W rules, based on the composition analysis by Speak et al. [19]. In reality, the lithium grease components of PE4 will contain a wide variety of hydrocarbon chain lengths, but as the heats of reaction and molar masses of these molecules scale proportionally to their chain length the error introduced with an assumption of $C_{25}H_{52}$ should be small. An MSDS for PE10 lists only PETN, mineral oil, and DMDNB as components, and so it is also modelled with paraffin wax. PE8 is RDX-based and uses a binder primarily formed from dioctyl sebacate (DOS) [20]. Using these simplified compositions, the approximate oxygen balances of the three plastic explosives are -84% for PE4, -78% for PE8 and -69% for PE10. The combustion reactions and heats for the paraffin wax and

Table 1: Simplified compositions of the considered plastic explosives.

Plastic Explosive	Explosive	Explosive fraction	Binder	Binder fraction
PE4	RDX	0.87	Paraffin wax	0.13
PE8	RDX	0.87	Dioctyl sebacate	0.13
PE10	PETN	0.84	Paraffin wax	0.16

Table 2: Detonation products and heat of detonation of RDX and PETN assuming Kistiakowsky–Wilson (K–W) rules.

Component	Formula	Molar mass (g/mol)	Detonation Products (K–W)	Heat of detonation (kJ/kg)
RDX	$C_3H_6N_6O_6$	222.117	$3\,CO + 3\,H_2O + 3\,N_2$	-5075
PETN	$C_5H_8N_4O_{12}$	316.138	$3\,CO_2 + 4\,H_2O + 2\,CO + 2\,N_2$	-5815

DOS are shown in Table 3.

In the absence of atmospheric oxygen, such as in inert nitrogen and argon atmospheres, combustion of the binder cannot occur. Long-chain hydrocarbons in inert atmospheres are known to decompose at elevated temperatures through pyrolysis reactions, producing a variety of smaller molecules [21, 22]. These reactions will have an associated heat of pyrolysis, but the products may also significantly affect the heat capacity of the overall atmosphere, affecting the overpressures generated. Gas chromatography of the final atmospheres in the PE4 experiments by Speak et al. [19] showed that detonation in an inert nitrogen atmosphere resulted in the formation of methane, CH_4, and soot, which was not present in the air atmosphere testing. These findings have been used to define simple pyrolysis reactions for the two binder materials, as shown in Table 4, along with their associated heat of pyrolysis.

Table 3: Heat of combustion and heat of afterburn for the explosives and binders.

Component	Formula	Molar mass (g/mol)	Combustion products	Heat of combustion (kJ/kg)	Heat of afterburn (kJ/kg)
RDX	$C_3H_6N_6O_6$	222.117	$3\,CO_2 + 3\,H_2O + 3\,N_2 - 1.5\,O_2$	-8898	-3822
PETN	$C_5H_8N_4O_{12}$	316.138	$5\,CO_2 + 4\,H_2O + 2\,N_2 - O_2$	-7605	-1790
Paraffin wax	$C_{25}H_{52}$	352.67	$25\,CO_2 + 26\,H_2O - 38\,O_2$	-42000	(-42000)
Dioctyl sebacate	$C_{26}H_{50}O_4$	426.68	$26\,CO_2 + 25\,H_2O - 36.5\,O_2$	-49186	(-49186)

Table 4: Heats of pyrolysis for binder materials in inert atmospheres for different assumptions of pyrolysis products: methane (CH_4); methane and ethylene (C_2H_4).

Component	Formula	Pyrolysis products	Heat of pyrolysis (kJ/kg)
Paraffin wax	$C_{25}H_{52}$	$13\,CH_4 + 12\,C$	-706
		$7\,C_2H_4 + 6\,CH_4 + 5\,C$	1846
Dioctyl sebacate	$C_{26}H_{50}O_4$	$12.5\,CH_4 + 4\,CO + 9.5\,C$	-737
		$6.5\,C_2H_4 + 6\,CH_4 + 4\,CO + 3\,C$	1222

Table 5: Initial mole fractions of the atmospheric gases used to model the QSP tests carried out by Farrimond et al. [17]. Air composition from Lemmon et al. [24].

Atmosphere	N_2	H_2O	CO	CO_2	O_2	Ar	C	CH_4
Air	0.7808	0	0	0.0004	0.2095	0.0093	0	0
Nitrogen	1	0	0	0	0	0	0	0
Argon	0	0	0	0	0	1	0	0

3. Thermochemical model

Now that the assumed explosive reactions are defined, the thermochemical model can be described. The model calculations can be summarised as follows:

1. The initial internal energy of the atmosphere in the confined volume;
2. The reaction products and energy release due to detonation, and afterburn as allowed by the atmospheric oxygen;
3. The temperature change in the final gas mixture based on the change in its internal energy and its heat capacity, and the resulting pressure change (QSP).

These calculations assume an ideal gas equation of state, the use of which is supported by the confined testing of plastic explosives carried out by Farrimond et al. [17]. The formulae below are shown in a similar vector format to those used in the accompanying Python script, `thermochemical_qsp.py` [23], to aid comparison.

3.1. Initial atmosphere moles and energy

The initial moles of gas in the atmosphere, $n_{\mathrm{atm},0}$, are calculated as

$$n_{\mathrm{atm},0} = \frac{P_0 \cdot V}{R \cdot T_0} \tag{2}$$

where P_0 and T_0 are the initial pressure (Pa) and temperature (K) inside a chamber of volume V (m^3), and $R = 8.314$ J/mol K is the gas constant. The vector $\boldsymbol{x}_{\mathrm{atm},0}$ contains the initial mole fractions of the component gases in the chamber

$$\boldsymbol{x}_{\mathrm{atm},0} = \Big[x(\mathrm{N_2}),\quad x(\mathrm{H_2O}),\quad x(\mathrm{CO}),\quad x(\mathrm{CO_2}),\quad x(\mathrm{O_2}),\quad x(\mathrm{Ar}),\quad x(\mathrm{C}),\quad x(\mathrm{CH_4})\Big] \tag{3}$$

where e.g. $x(\mathrm{N_2})$ is the mole fraction of nitrogen. The values of $\boldsymbol{x}_{\mathrm{atm},0}$ used for the air, nitrogen and argon atmospheres in this paper are shown in Table 5. The initial moles of each gas are then calculated as

$$\boldsymbol{n}_{\mathrm{atm},0} = \boldsymbol{x}_{\mathrm{atm},0} \cdot n_{\mathrm{atm},0} \tag{4}$$

where the vector $\boldsymbol{n}_{\mathrm{atm},0}$ similarly has the form

$$\boldsymbol{n}_{\mathrm{atm},0} = \Big[n(\mathrm{N_2}),\quad n(\mathrm{H_2O}),\quad n(\mathrm{CO}),\quad n(\mathrm{CO_2}),\quad n(\mathrm{O_2}),\quad n(\mathrm{Ar}),\quad n(\mathrm{C}),\quad n(\mathrm{CH_4})\Big]. \tag{5}$$

The initial internal energy of the chamber gases, $U_{\mathrm{atm},0}$, is

$$U_{\mathrm{atm},0} = C_{v,\mathrm{atm},0} \cdot n_{\mathrm{atm},0} \cdot T_0 \tag{6}$$

where $C_{v,\mathrm{atm},0}$ is the heat capacity at constant volume for the initial gas mixture.

3.2. Products and energy release

The moles of explosive and binder in the charge before detonation can be calculated as

$$n_{\mathrm{exp}} = m_{\mathrm{exp}}/M_{\mathrm{exp}} \tag{7}$$

$$n_{\mathrm{bin}} = m_{\mathrm{bin}}/M_{\mathrm{bin}} \tag{8}$$

where m and M are the mass and molar mass in each case, using the component ratios in Table 1 and the molar masses in Table 3. The vectors $\boldsymbol{x}_{\text{exp,det}}$, $\boldsymbol{x}_{\text{exp,ab}}$, $\boldsymbol{x}_{\text{bin,ab}}$ and $\boldsymbol{x}_{\text{bin,pyro}}$ contain the coefficients of the gaseous products for the explosive detonation, explosive afterburn, binder afterburn, and binder pyrolysis respectively. Each vector has the general form of Equation 3, using the values shown in Tables 2 and 3: afterburn products for the explosives are calculated as the difference between the products for full combustion and for detonation. Negative coefficients for oxygen indicate reactions where an external source of oxygen is required.

Assuming that there is sufficient oxygen for all reactions to continue to completion, the moles of gaseous products in the explosive detonation, explosive afterburn, and binder afterburn could be calculated as

$$\boldsymbol{n}_{\text{exp,det}} = \boldsymbol{x}_{\text{exp,det}} \cdot n_{\text{exp}} \tag{9}$$

$$\boldsymbol{n}_{\text{exp,ab}} = \boldsymbol{x}_{\text{exp,ab}} \cdot n_{\text{exp}} \tag{10}$$

$$\boldsymbol{n}_{\text{bin,ab}} = \boldsymbol{x}_{\text{bin,ab}} \cdot n_{\text{bin}} \tag{11}$$

where again the vectors $\boldsymbol{n}_{\text{exp,det}}$, $\boldsymbol{n}_{\text{exp,ab}}$ and $\boldsymbol{n}_{\text{bin,ab}}$ have the form of Equation 5. The maximum extent to which afterburn can occur is controlled by the ratio of oxygen available in the atmosphere immediately after detonation to the oxygen required for complete afterburn of the explosive and binder. This is expressed using the afterburn ratio β,

$$\beta = \min\left(\frac{n(\mathrm{O_2})_{\text{atm,0}} + n(\mathrm{O_2})_{\text{exp,det}}}{|n(\mathrm{O_2})_{\text{exp,ab}} + n(\mathrm{O_2})_{\text{bin,ab}}|}, 1\right) \tag{12}$$

where the maximum value of 1 indicates full combustion of the explosives and binder. This simple relationship assumes that there is sufficient mixing

of the detonation products with the atmospheric oxygen while the detonation products remain hot enough to combust, so that all of the oxygen available for afterburn reacts successfully. This may not be the case in some situations, such as at low levels of atmospheric oxygen, where the reactions may freeze out before full combustion is achieved. Assuming that afterburn proceeds based on the total availability of oxygen, and that uncombusted binder undergoes pyrolysis instead, the final number of moles of each component gas in the chamber atmosphere is

$$\boldsymbol{n}_{\mathrm{atm},1} = \boldsymbol{n}_{\mathrm{atm},0} + \boldsymbol{n}_{\mathrm{exp,det}} + \beta\boldsymbol{n}_{\mathrm{exp,ab}} + \beta\boldsymbol{n}_{\mathrm{bin,ab}} + (1-\beta)\boldsymbol{n}_{\mathrm{bin,pyro}} \tag{13}$$

where $\boldsymbol{n}_{\mathrm{bin,pyro}} = \boldsymbol{x}_{\mathrm{bin,pyro}} \cdot n_{\mathrm{bin}}$. The internal energy of the gases in the chamber as a result of these reactions is then

$$\begin{aligned} U_{\mathrm{atm},1} = U_{\mathrm{atm},0} - m_{\mathrm{exp}}\Delta H_{\mathrm{exp,det}} - \beta m_{\mathrm{exp}}\Delta H_{\mathrm{exp,ab}} \\ - \beta m_{\mathrm{bin}}\Delta H_{\mathrm{bin,ab}} - (1-\beta)m_{\mathrm{bin}}\Delta H_{\mathrm{bin,pyro}} \end{aligned} \tag{14}$$

where $\Delta H_{\mathrm{exp,det}}$ is the heat of detonation of the explosive from Table 2, $\Delta H_{\mathrm{exp,ab}}$ and $\Delta H_{\mathrm{bin,ab}}$ are the heats of combustion for the detonation products and the binder, or the 'heat of afterburn', as listed in Table 3, and $\Delta H_{\mathrm{bin,pyro}}$ is the heat of pyrolysis as listed in Table 4.

3.3. Temperature and pressure change

The change in the internal energy of the gases, ΔU, will result in a change of temperature, ΔT, and in turn a change in gas pressure, ΔP, in the chamber. The temperature change in a gas under constant volume conditions depends on its molar heat capacity at constant volume, C_v, which itself is

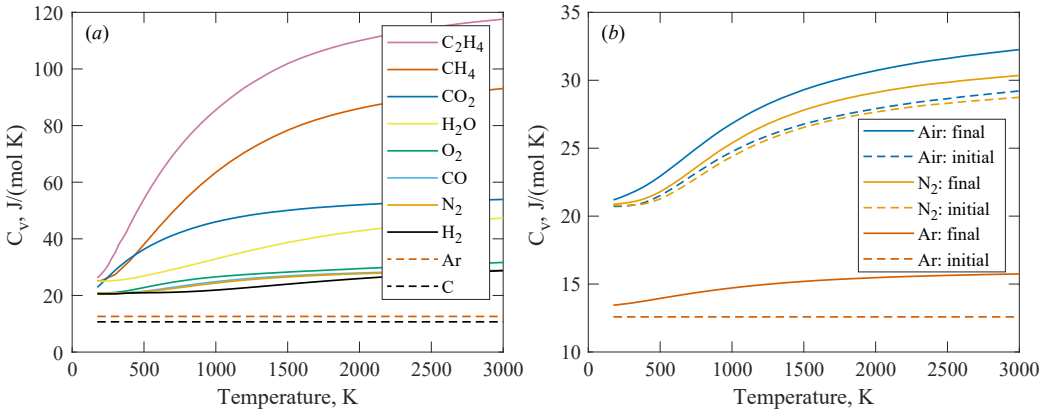

Figure 3: Relationship between temperature and the molar heat capacity at constant volume of (a) the individual atmospheric gases and reaction products [25], and (b) the initial and predicted final gas mixture in a 275L blast chamber for the detonation of a 30g PE10 charge in air, nitrogen and argon atmospheres.

dependent on temperature:

$$\Delta U = C_v(T) n \Delta T. \tag{15}$$

The molar heat capacities for the individual atmospheric gases and products are shown in Figure 3a. In a mixture of gases, this relationship can be expressed using the mean of the gas heat capacities, each weighted by their mole fraction,

$$C_{v,\text{mix}}(T) = \frac{\sum_i n_i \cdot C_{v,i}(T)}{\sum_i n_i} \tag{16}$$

where n_i and $C_{v,i}(T)$ are the number of moles and the heat capacities of each constituent gas. Calculating this mole-weighted heat capacity for $\boldsymbol{n}_{\text{atm},1}$ and substituting in Equation 15 defines a relationship in terms of internal energy and temperature: as the final internal energy $U_{\text{atm},1}$ is known, this can be solved numerically to find the final temperature, T_1. The final pressure in

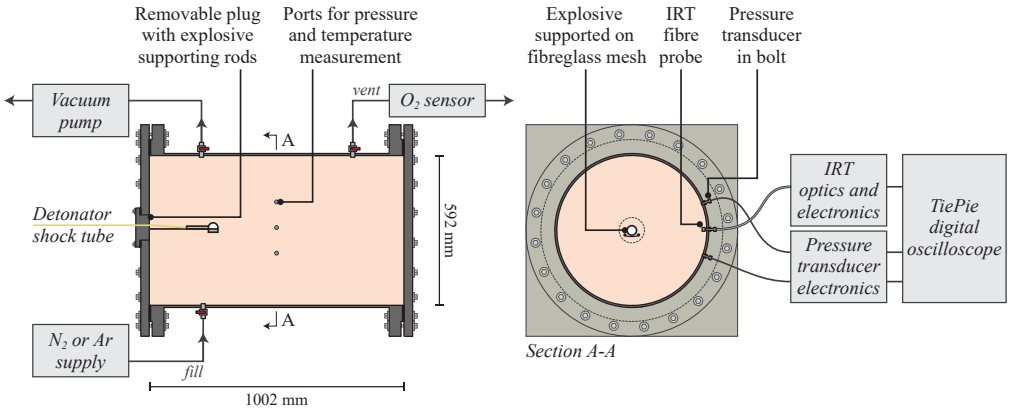

Figure 4: The 275L confined blast chamber used by Farrimond et al. [17], which incorporated control over atmospheric gases and high-speed measurement of pressure and temperature.

the chamber can then be calculated using the ideal gas law as

$$P_1 = \frac{\sum_i n_{\mathrm{atm},1,i} \cdot R \cdot T_1}{V} \tag{17}$$

with the quasi-static pressure above ambient conditions equalling

$$P_{\mathrm{qsp}} = P_1 - P_0. \tag{18}$$

4. Experimental validation

In order to assess the performance of this simplified model, thermochemical predictions are compared with the temperature and pressure measurements recorded by Farrimond et al. [17] using the 275L confined blast chamber shown in Figure 4. The walls of this 1m long steel pipe were fitted with pressure transducers to measure QSP, and a high-speed infrared thermometer to record temperature. Valves in the chamber wall were also used to control the initial atmosphere, with the ability to evacuate the chamber and fill with

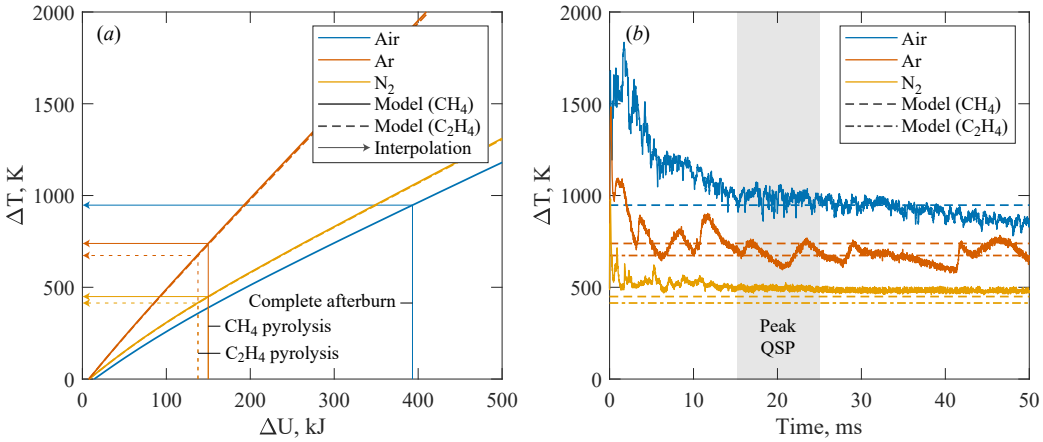

Figure 5: (a) An illustration of how the thermochemical model uses the energy release and mole-weighted heat capacities to calculate the temperature change of the chamber gases, for 30g PE10 charges in air, argon and nitrogen atmospheres. (b) A comparison of the model temperature predictions against experimental measurements made using a high speed infrared thermometer [17]. Predictions in inert atmospheres are shown using assumed pyrolysis reactions with methane (CH_4) or methane and ethylene (C_2H_4).

bottled gases such as nitrogen and argon. In these experiments the chamber was unvented and gas-tight, and so any decay of the internal pressure after peak QSP was reached was shown to be due to heat loss to the chamber walls. The initial ambient atmospheric conditions in these experiments were $P_0 = 97.0$kPa and $T_0 = 280$K, with $V = 0.275\text{m}^3$.

4.1. Model predictions of temperature

Farrimond et al.'s [17] experiments incorporated a high-speed infrared thermometer (IRT) to record detonation product temperatures inside the chamber. This was built around a Si–InGaAs two-colour photodiode with a response time of under 1μs, and was connected to the chamber using a silica fibre optic probe in a protective bolt assembly [26], allowing an assessment

of the thermochemical model's predictions of temperature change. Figure 5a provides a visual representation of Equation 15 and the model's calculation of the temperature change resulting from detonations of 30g PE10 in air, nitrogen and argon atmospheres. In each case, the curved lines represent the temperature-dependent mole-weighted heat capacities, $C_{v,\mathrm{mix}}(T)$, of the final chamber atmospheres after detonation. The combined heats of detonation, combustion and/or pyrolysis define the change in internal energy, ΔU, and an interpolation of the $C_{v,\mathrm{mix}}(T)$ curve provides the predicted change in temperature, ΔT.

As a monatomic gas, the heat capacity of argon is much lower than that of nitrogen and air, and is temperature independent (Figure 3b). As a result, the curve in Figure 5a is much steeper for detonations in argon than in air and nitrogen, and the assumptions of combustion and pyrolysis reactions will have a larger effect in an argon atmosphere than in nitrogen. For example, methane and simple atomic carbon soot have been assumed as pyrolysis products in the model, but the decomposition of long hydrocarbons often produces a wide range of products, including both alkanes and alkenes. The concentration of these products is also sensitive to the temperature at which thermal decomposition takes place [21]. To demonstrate the sensitivity of the monatomic argon atmosphere to the assumed pyrolysis reactions, a further example is provided where it is assumed that the simplest alkene (ethylene, C_2H_4) is produced alongside the simplest alkane (methane, CH_4). Ethylene was not recorded in Speak et al.'s analysis [19] of the products in a nitrogen atmosphere, but would not be visible using the method used as C_2H_4 has a similar molar mass to both N_2 and CO. The production of ethylene is

endothermic (Table 4), and so this assumption reduces the predicted temperature change in Figure 5a—by 66K in an argon atmosphere, and by 35K in nitrogen.

Figure 5b shows the temperature changes recorded experimentally using the IRT over the first 50ms. Unlike the pressure transducers, which record the pressure at a point on the chamber wall, the IRT probe has a field of view over a significant volume of the chamber interior. The large temperature spikes in the first 10ms are theorised by Farrimond et al. to be due to the flame temperature of the initial fireball, and to subsequent afterburn reactions in the case of the air atmosphere. The temperatures in all three atmospheres reach a steady state by approximately 20ms, which correlates with the timing of the peak QSPs measured using the pressure transducers. At this point, the temperature changes predicted by the model agree well with the experimental measurements of temperature, indicating that the assumption of ideal gas behaviour is valid at the point that peak QSP is achieved. This finding aligns with Cooper's [27] assertion that an ideal gas EOS will closely approximate gas behaviours in confined detonations up to 20,000 kPa and 4000°C and so, for typical public safety scenarios, the ideal gas simplification can be made with some confidence.

Detonation in a nitrogen atmosphere appears to be best represented using the proposed pyrolysis reaction with methane and carbon, while the prediction in the argon atmosphere is improved by the addition of ethylene to the pyrolysis products.

Table 6: Experimental peak QSP data for PE10 charges in air compared with the simplified thermochemical model and UFC 3-340-02 predictions.

Charge mass (g)	Experimental peak QSP (kPa)	Thermochemical prediction (kPa)	Error (%)	UFC 3-340-02 prediction (kPa)	Error (%)
10	156	158	1	176	13
20	292	284	-3	304	4
30	397	399	1	427	8
40	491	508	3	539	10
50	611	612	0	650	6

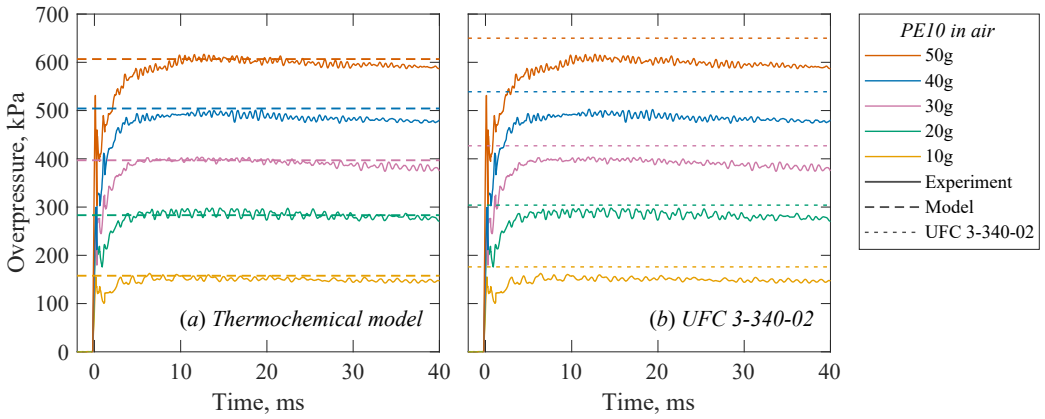

Figure 6: Comparison of experimental data and predicted peak QSP for masses of PE10 between 10g and 50g in air (a) using the thermochemical model, and (b) using the UFC 3-340-02 empirical method [10].

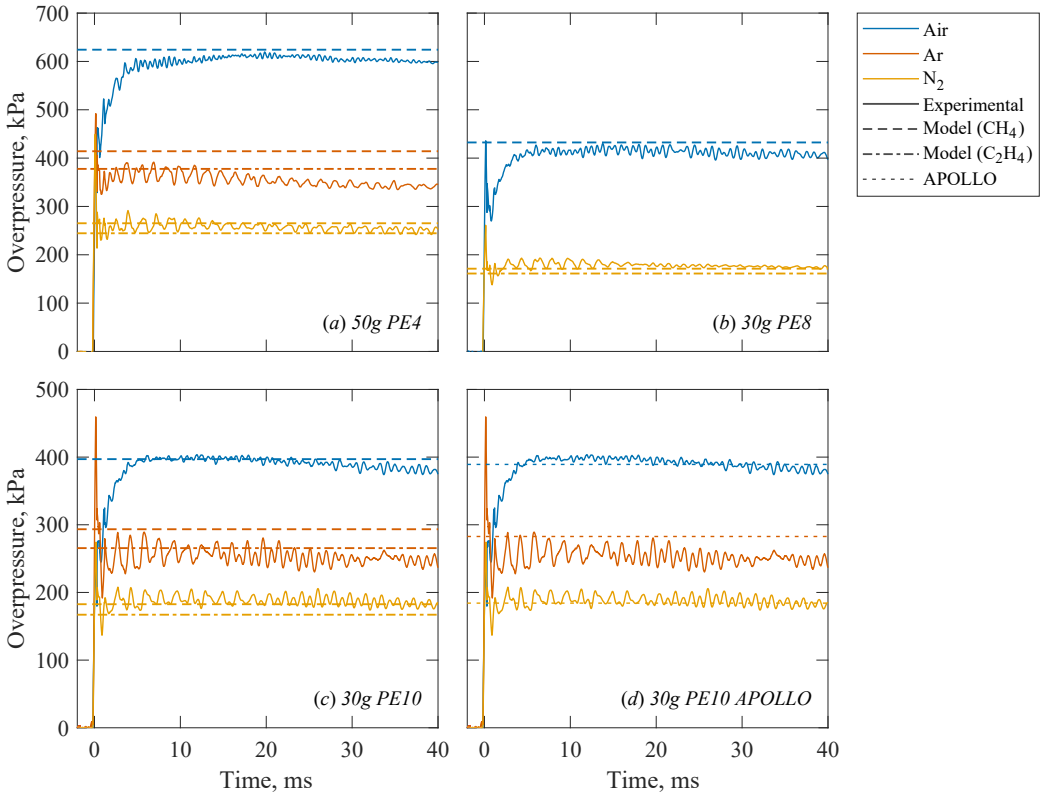

Figure 7: Comparison of experimental data and predicted peak QSP using the thermochemical model for (a) 50g PE4 in air, argon and nitrogen atmospheres, (b) 30g PE8 in air and nitrogen atmospheres, and (c) 30g PE10 in air, argon and nitrogen atmospheres. Predictions in inert atmospheres are shown using assumed pyrolysis reactions with methane (CH_4) or methane and ethylene (C_2H_4). (d) Comparisons of experimental data and APOLLO blastsimulator CFD predictions of peak QSP for 30g PE10 in air, argon and nitrogen atmospheres [17].

4.2. Model predictions of pressure

Table 6 and Figure 6a show the experimental overpressure data for spherical charges of PE10 in an air atmosphere, where the charge mass varies between 10g and 50g. The oxygen available in the chamber atmosphere in these experiments varies from approximately 1200% to 240% of the moles required for full combustion of the detonation products and binder. Figure 6a shows the time-dependent smoothed average of the raw pressure signals, which emphasises the apparent quasi-static pressure in the chamber rather than the individual shock reflections that dominate the signal over approximately the first 100ms [2]. The thermochemical model successfully predicts the peak QSP to within 3% of the experimental value in each case, indicating that the simplifying assumptions made around the binder formulation and detonation/afterburn reactions are suitable for plastic explosives in oxygenated atmospheres.

By comparison, the UFC 3-340-02 values in Table 6 and Figure 6b overpredict the experimental results by up to 13%. These UFC 3-340-02 values were calculated from Figure 1 and Equation 1 using the same assumptions on explosive formulation discussed above. The heats of detonation and combustion for the explosive and binder were each factored by their respective mass fractions to define the TNT equivalence of the plastic explosive, and the empirical curve was interpolated numerically to achieve as representative a reading as possible.

Figures 7a–c show experiments with PE4, PE8 and PE10 charges detonated in air, argon and nitrogen atmospheres. Thermochemical model predictions of peak QSP in both the air and nitrogen atmospheres are within

3% of the experimental results for all three plastic explosives, showing that the relative contributions of detonation and afterburn are reliably captured in oxygenated and inert atmospheres for a variety of explosive and binder types. Figure 7d also includes the peak QSP predicted for 30g PE10 charges using a CFD analysis with APOLLO blastsimulator, which used an explosive equation of state derived from the CHEETAH and EXPLO5 thermochemical codes [17, 28]. These simulations did not account for heat loss to the chamber walls, and so peak QSP values have been taken from the time-dependent smoothed average of the APOLLO results at 20ms: this corresponds to the point in the experimental results where peak QSP has been achieved, but pressure decay due to heat loss is not yet evident. The CFD model results are also within 4% of the experimental values for the air and nitrogen atmospheres.

Peak pressures for the PE4 and PE10 charges in an argon atmosphere are overpredicted by the model by around 14% when using methane and carbon as pyrolysis products, and are also overpredicted by 10% when performing a CFD analysis in APOLLO. It was noted above that the temperature change in argon atmospheres was better represented when ethylene was included in the pyrolysis reaction products, and this is also the case for pressure: thermochemical model predictions of QSP for PE4 and PE10 are within 4% of the experimental results when ethylene is included. The thermochemical model code accompanying this paper has been provided with the methane–carbon assumption for binder pyrolysis in the three explosives, as this is shown to be accurate for the air and nitrogen atmospheres which are likely to be more appropriate in most partially-oxygenated use cases. The model's conserva-

tive prediction for argon atmospheres also remains useful, as consideration of different atmospheric gases is not a feature of existing empirical methods, which are solely based on detonations in air.

5. Model behaviour with W/V ratio

An immediate prediction of QSP can be made using the Python function `thermochemical_qsp()` [23], which implements the methodology outlined in the preceding sections. The function syntax is `thermochemical_qsp(mass, explosive_type, volume, atmosphere)`, where `mass` defines the explosive mass in kg, `explosive_type` is currently defined for PE4, PE8 and PE10, `volume` defines the confined volume in m^3, and `atmosphere` is the initial gas mixture, currently defined for air, nitrogen and argon. The initial pressure and temperature of the atmosphere may also be specified.

Figures 8a–c show the model predictions across a range of W/V (charge mass/volume) ratios in both air and nitrogen atmospheres for the three plastic explosives considered. In each case, the effects of afterburn in the oxygen-rich air atmosphere result in a significantly higher peak QSP than in the inert nitrogen atmosphere. This trend continues with increasing charge mass until there are insufficient moles of oxygen to fully combust all of the reaction products. From this point on, partial afterburn and pyrolysis occur as allowed by the available oxygen, and the peak QSP predictions begin to converge with those for the inert atmosphere as W/V continues to rise, as is expected.

Also shown in Figures 8a–c is the UFC 3-340-02 prediction for each explosive, using the empirical TNT data in Figure 1 along with the TNT equivalence factor in Equation 1. As noted above, implementing this equivalence

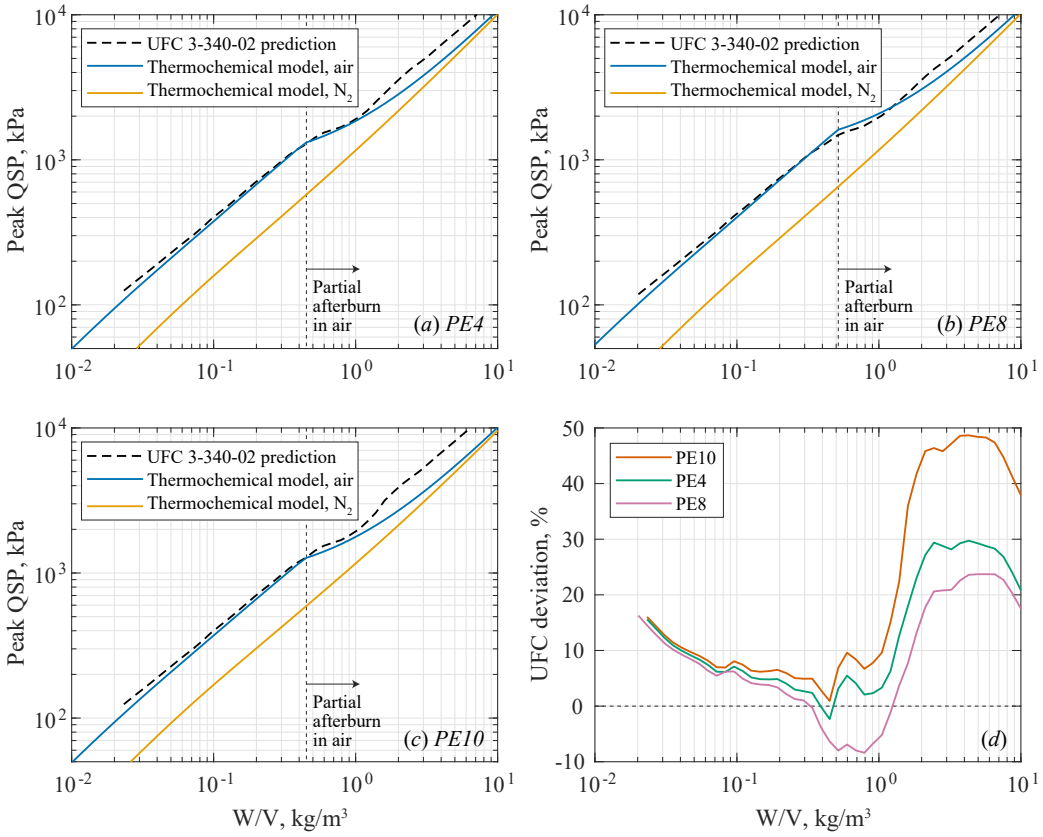

Figure 8: Thermochemical model predictions in air and nitrogen atmospheres and comparison with UFC 3-340-02 empirical method [10] for a) PE4, b) PE8 and c) PE10. d) The deviation of the UFC prediction from the thermochemical model for each explosive, as a function of W/V ratio.

factor requires the same assumptions on explosive formulation and heats of detonation and combustion as the thermochemical method, but simply applies the resulting value as a factor to the empirical TNT curve. In the region of complete afterburn, deviation of the UFC predictions from the thermochemical model is of a similar level to the error observed in comparison with the experimental data, with a deviation of 16% at the smallest W/V ratio defined on the UFC curve. This deviation decreases as the explosive mass increases, but then quickly increases again to a 25–50% overprediction in the region of partial afterburn, as shown in Figure 8d. In this region the UFC prediction does not converge with the inert atmosphere case as expected. This is likely because Equation 1 reduces to a ratio of the heats of detonation at higher W/V ratios, and cannot account for the effects of a non-detonating binder on the energy release and the heat capacity of the final gas mixture. Edri et al. [16] also noted the limitations of the UFC TNT equivalence method in their analysis of simpler single-component explosives such as RDX and PETN: in order to reduce the observed errors a new ϕ function (Figure 1b) had to be defined for each new explosive.

An additional benefit of the thermochemical analysis method is that variations in the initial conditions can be taken into account. The pressure and temperature of the initial gas mixture will directly affect the initial moles of gas in the enclosed volume (Equation 2), and hence also the moles of oxygen available. The effect of varying the initial pressure and temperature is shown in Figure 9 for the case of PE10. Within normal ranges, e.g. $95 \leq P_0 \leq 105$ kPa and $273 \leq T_0 \leq 300$ K, this effect is very small, and only slightly affects the onset of partial afterburn. However, significantly higher initial pressures,

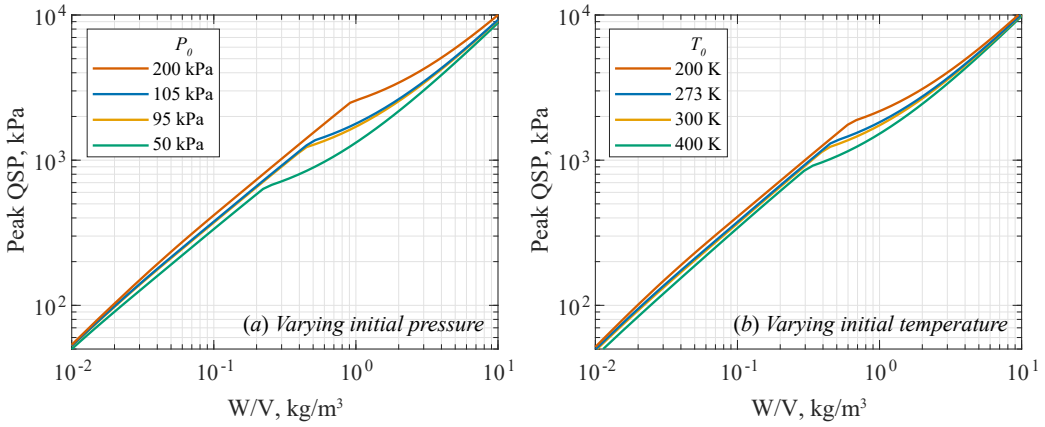

Figure 9: Thermochemical model sensitivity to changes in a) initial atmospheric pressure, P_0 at $T_0 = 273$ K, and b) initial atmospheric temperature, T_0 at $P_0 = 100$ kPa, for PE10 detonations in air.

or significantly lower initial temperatures, allow complete afterburn to occur at higher W/V ratios as a result of the increased total oxygen in the initial atmosphere. There is also a noticeable increase in peak QSP at all W/V ratios, as the final mean heat capacity of the gas mixture is reduced due to the high heat capacity detonation/combustion products making up a lower proportion of the total moles in the space (e.g. see CO_2 and H_2O in Figure 3a). Likewise, significantly lower initial pressures and higher initial temperatures result in a noticeable decrease in peak QSP and an earlier onset of partial afterburn due to the increased heat capacity of the final atmosphere and decreased oxygen availability. The significance of these effects will vary based on both the initial atmosphere and the explosive, but as they are automatically taken into account by the model, the resulting predictions should remain valid over a wide range of initial conditions.

6. Conclusions

In this paper we have developed a thermochemical model for the quasi-static pressure (QSP) generated by confined detonations of plastic explosives in oxygenated and inert atmospheres, seeking to overcome the limitations of existing empirical methods. This model considers the chemical products and energy release of the detonation and combustion reactions, and uses an assumption of ideal gas behaviour to calculate the resultant temperature and pressure change in a fixed volume. Recognising the variability and complexity of plastic explosive mixtures, simplifying assumptions were made on the binder chemistry and reactions based on chemical analyses of the explosives and their reaction products, including thermal decomposition of the binders in inert atmospheres.

The thermochemical model was validated against experimental measurements of QSP from PE4, PE8 and PE10 detonations in a 275L chamber filled with air, nitrogen and argon atmospheres. Temperature changes predicted by the model agreed well with high-speed infrared thermometer measurements at the point of peak QSP, indicating that the ideal gas assumptions are valid for QSP prediction. The thermochemical model produces excellent predictions of peak QSP when compared to the experimental data for air and nitrogen, with deviations below 3% across all explosives at a range of masses. These results indicate that the simplifying assumptions on products and heats of reactions suitably capture the contributions of detonation and afterburn in both oxygenated and inert atmospheres, for a variety of explosive and binder combinations. Detonations in an argon atmosphere are particularly sensitive to the assumed pyrolysis products due to the monatomic gas's

low heat capacity, and the thermochemical model initially overpredicted QSP by up to 14%; the inclusion of ethylene in the pyrolysis products returned the predictions to within 4% of the experimental values.

The thermochemical model is intended to improve on existing empirical methods while acting as a fast-running alternative to more complex CFD methods, and so its performance was also compared against the UFC 3-340-02 curves and modelling in APOLLO blastsimulator. The UFC 3-340-02 method is limited to predictions in air at standard temperature and pressure, and consistently overpredicted the peak QSP in air by up to 13% compared to the experimental values, despite making the same simplifying assumptions on explosive formulation and heats of reaction. Larger errors of around 25% to 50% were also observed in the UFC method at higher W/V ratios, as the simple TNT equivalence method does account for the effect of non-detonating materials such as binders. As well as outperforming the empirical method, the thermochemical model also compared favourably to CFD simulations in air, argon and nitrogen atmospheres, achieving similar or lower errors on peak QSP without the requirement to model the event geometry or define explosive equations of state. These advanced methods will however remain useful for scenarios where a time-resolved analysis of pressure development is required for specific points in a space, especially for more complex internal geometries.

The model described in this paper is provided as an open source Python script for further development. The fast-running nature of this model makes it suitable for the swift evaluation of multiple explosive scenarios, providing a valuable alternative to more detailed thermochemical codes and CFD meth-

ods during the preliminary design of structures, or the rapid assessment of explosive devices by government agencies when a threat is not well characterised. The model can be readily adapted for new explosive formulations and atmospheric conditions, and has the potential to include additional reactions, such as the afterburn in aluminised explosives, the response of mitigating materials on QSP generation, and the effects of heat transfer and venting on the pressure decay following the peak.

Funding

This work was funded by the Engineering and Physical Sciences Research Council (ESPRC) as part of the Mechanisms and Characterisation of Explosions (MaCE) project, EP/R045240/1.

References

[1] D. J. Pope, The development of a quick-running prediction tool for the assessment of human injury owing to terrorist attack within crowded metropolitan environments, Philosophical Transactions of the Royal Society B: Biological Sciences 366 (1562) (2011) 127–143.

[2] A. L. Kuhl, J. Forbes, J. Chandler, A. K. Oppenheim, R. Spektor, R. E. Ferguson, Confined combustion of tnt explosion products in air, Tech. Rep. - LLNL Report: UCRL-JC-131748, Lawrence Livermore National Laboratory, Livermore, CA, USA (1998).

[3] D. L. Ornellas, Calorimetric determinations of the heat and products of detonation for explosives: October 1961 to april 1982, Tech. rep., Lawrence Livermore National Laboratory (1982).

[4] P. Wolanski, Z. Gut, W. A. Trzcinski, L. Szymanczyj, J. Paszula, Visualization of turbulent combustion of tnt detonation products in a steel vessele, Shock Waves 10 (2000) 127–136.

[5] H. R. Weibull, Pressures recorded in partially closed chambers at explosion of TNT charges., Annals of the New york Academy of Sciences 152 (1) (1968) 357–361.

[6] C. N. Kingery, R. Schumacher, W. Ewing, Internal pressure from explosions in suppressive structures, Tech. rep., USA Ballistic Research Laboratories, Aberdeen Proving Ground, Maryland (1978).

[7] G. F. Kinney, E. Sewell, Venting of explosions, Naval Weapons Center, China Lake, California, 1974.

[8] E. Esparza, W. Baker, G. Oldham, Blast pressures inside and outside suppressive structures, Department of the Army, Edgewood Arsenal, 1975.

[9] C. E. Anderson Jr, W. Baker, D. K. Wauters, B. L. Morris, Quasi-static pressure, duration, and impulse for explosions (eg he) in structures, International Journal of Mechanical Sciences 25 (6) (1983) 455–464.

[10] US Department of Defence, Structures To Resist the Effects of Accidental ExplosionsUFC 3-340-02. US DoD, Washington, DC (2008).

[11] Z. Wei, T. Zhou, Calculation of quasi-static pressures for confined explosions considering chemical reactions under isobaric assumption., Explosion Shock Waves S1 (2013) 78–83.

[12] L. Donahue, F. Zhang, R. Ripley, Numerical models for afterburning of tnt detonation products in air, Shock Waves 23 (2013) 559–573.

[13] L. Fried, P. Souers, Cheetah: A next generation thermochemical code, Tech. rep., Lawrence Livermore National Lab.(LLNL), Livermore, CA (United States) (1994).

[14] W. A. Trzciński, J. Paszula, P. Wolański, Thermodynamic analysis of afterburning of detonation products in confined explosions, Journal of Energetic Materials 20 (3) (2002) 195–222.

[15] V. R. Feldgun, Y. S. Karinski, I. E. Edri, D. Z. Yankelevsky, Prediction of the quasi-static pressure in confined and partially confined explosions and its application to blast response simulation of flexible structures, International Journal of Impact Engineering 90 (2016) 46–60.

[16] I. E. Edri, H. Y. Grisaro, D. Z. Yankelevsky, Tnt equivalency in an internal explosion event, Journal of Hazardous Materials 374 (2019) 248–257.

[17] D. Farrimond, S. Woolford, A. Barr, T. Lodge, A. Tyas, R. Waddoups, S. Clarke, S. Rigby, M. Hobbs, J. Willmott, M. Whittaker, D. Pope, M. Handy, Experimental studies of confined detonations of plasticised high explosives in inert and reactive atmospheres, Proceedings of the Royal Society A 480 (20240061) (2024).

[18] J. Akhavan, The chemistry of explosives, Royal Society of Chemistry, 2011.

[19] T. Speak, S. Woolford, D. Farrimond, I. Christopher, A. Barr, P. Portius, A. Tyas, Experimental observation and modelling of contained detonations of pe4: What is the influence of afterburn?, in: 2022 International Explosives Conference, London, 2022.

[20] G. O. Nevstad, Determination of detonation velocity and plate dent properties of dpx-9 and dpx-10, Tech. rep., Norwegian Defence Research Establishment (2009).

[21] E. Ranzi, A. Frassoldati, S. Granata, T. Faravelli, Wide-range kinetic modeling study of the pyrolysis, partial oxidation, and combustion of heavy n-alkanes, Industrial & engineering chemistry research 44 (14) (2005) 5170–5183.

[22] F. Cammarota, A. Di Benedetto, V. Di Sarli, E. Salzano, Influence of initial temperature and pressure on the explosion behavior of n-dodecane/air mixtures, Journal of Loss Prevention in the Process Industries 62 (2019) 103920.

[23] A. Barr, thermochemical_qsp.py - a fast-running thermochemical model for predictions of quasi-static pressure for confined detonations of plasticised high explosives (2025). doi:10.15131/shef.data.29649125.
URL `https://doi.org/10.15131/shef.data.29649125`

[24] E. W. Lemmon, R. T. Jacobsen, S. G. Penoncello, D. G. Friend, Thermodynamic properties of air and mixtures of nitrogen, argon, and oxygen from 60 to 2000 k at pressures to 2000 mpa, Journal of physical and chemical reference data 29 (3) (2000) 331–385.

[25] P. Linstrom, W. Mallard, NIST Chemistry WebBook, NIST Standard Reference Database Number 69, National Institute of Standards and Technology, Gaithersburg MD. doi:10.18434/T4D303.

[26] M. J. Hobbs, A. Barr, S. Woolford, D. Farrimond, S. D. Clarke, A. Tyas, J. R. Willmott, High-speed infrared radiation thermometer for the investigation of early stage explosive development and fireball expansion, Sensors 22 (16) (2022) 6143.

[27] P. W. Cooper, Explosives Engineering, John Wiley & Sons, 1996.

[28] D. G. Farrimond, S. Woolford, A. Tyas, S. E. Rigby, S. D. Clarke, A. Barr, M. Whittaker, D. J. Pope, Far-field positive phase blast parameter characterisation of rdx and petn based explosives, International Journal of Protective Structures 15 (1) (2024) 141–165.